Published in final edited form as:
Nat Neurosci. 2013 August ; 16(8): 1032–1041. doi:10.1038/nn.3459.

Developmental origin dictates interneuron AMPA and NMDA receptor subunit composition and plasticity

Jose A Matta[1,2], **Kenneth A Pelkey**[1], **Michael T Craig**[1], **Ramesh Chittajallu**[1], **Brian W Jeffries**[1], and **Chris J McBain**[1]

[1]Program in Developmental Neurobiology, Eunice Kennedy-Shriver National Institute of Child Health and Human Development, National Institutes of Health, Bethesda, Maryland, USA

Abstract

Disrupted excitatory synapse maturation in GABAergic interneurons may promote neuropsychiatric disorders such as schizophrenia. However, establishing developmental programs for nascent synapses in GABAergic cells is confounded by their sparsity, heterogeneity and late acquisition of subtype-defining characteristics. We investigated synaptic development in mouse interneurons targeting cells by lineage from medial ganglionic eminence (MGE) or caudal ganglionic eminence (CGE) progenitors. MGE-derived interneuron synapses were dominated by GluA2-lacking AMPA-type glutamate receptors (AMPARs), with little contribution from NMDA-type receptors (NMDARs) throughout development. In contrast, CGE-derived cell synapses had large NMDAR components and used GluA2-containing AMPARs. In neonates, both MGE- and CGE-derived interneurons expressed primarily GluN2B subunit–containing NMDARs, which most CGE-derived interneurons retained into adulthood. However, MGE-derived interneuron NMDARs underwent a GluN2B-to-GluN2A switch that could be triggered acutely with repetitive synaptic activity. Our findings establish ganglionic eminence–dependent rules for early synaptic integration programs of distinct interneuron cohorts, including parvalbumin- and cholecystokinin-expressing basket cells.

Activity-driven refinement of nascent synaptic connections regulates circuit formation and development throughout the nervous system. Postsynaptically, many central excitatory synapses undergo stereotyped use-dependent developmental alterations in the relative proportion of synaptic input carried by AMPARs and NMDARs. In the extreme case, immature synapses proceed from being silent, with transmission mediated solely by NMDARs, to being functional through the stepwise acquisition of AMPARs[1]. Additional refinement is achieved by alterations in the molecular and biophysical characteristics of

Correspondence should be addressed to K.A.P. (pelkeyk2@mail.nih.gov).
[2]Present address: Janssen Research & Discovery, La Jolla, California, USA.

Note: Supplementary information is available in the online version of the paper.

AUTHOR CONTRIBUTIONS

J.A.M., K.A.P. and C.J.M. conceived of the project, designed experiments and wrote the manuscript. J.A.M., K.A.P., M.T.C. and R.C. conducted experiments and analyzed the data. B.W.J. provided technical assistance with cell recoveries and drawings. C.J.M. and K.A.P. supervised the project.

COMPETING FINANCIAL INTERESTS

The authors declare no competing financial interests.

these two primary mediators of fast excitatory transmission through changes in receptor subunit composition. For example, developmental increases in the ratio of GluA2 to other AMPAR subunits occur throughout the CNS concomitant with the removal of a transient population of GluA2-lacking AMPARs at various central synapses[2–4]. Similarly, a change in NMDAR subunit composition, with GluN2B-containing receptors dominating transmission during the first postnatal week that are then replaced with GluN2A-containing receptors during experience-driven synapse maturation, is conserved at diverse excitatory connections throughout the nervous system[5–10].

In the cortex, such developmental programs of synaptic refinement have been elucidated primarily at connections between principal glutamatergic neurons, as this population is a relatively homogenous cohort of numerically dominant neurons within forebrain circuits, which makes them readily accessible for repeated analyses at the population and single-cell levels. However, appropriate circuit formation also requires the network integration of a much smaller population of highly diverse inhibitory GABAergic interneurons. Though vastly outnumbered, interneurons shape circuit computation by pacing and synchronizing excitatory principal-cell activity[11]. Like principal cells, interneurons must be synaptically integrated into developing cortical circuits, which requires the appropriate formation and refinement of excitatory afferent drive onto these inhibitory cells. Indeed, deficits in AMPAR and NMDAR function in specific interneuron cohorts disrupts the coordination of principal-cell activity and may underlie developmentally regulated neurological disorders such as schizophrenia[12,13]. However, the sparse and heterogeneous nature of cortical GABAergic interneurons combined with their relatively late acquisition of subtype-defining cellular and molecular characteristics at postnatal weeks 2–3 has confounded the investigation of developmental rules governing the circuit integration properties of specific interneuron cohorts.

Despite their late postnatal phenotypic maturation, the ultimate fate adopted by a given cortical interneuron is determined largely at the progenitor stage during embryogenesis[14]. Both neocortical and hippocampal interneurons derive primarily from progenitors in the MGE and CGE of the ventral telencephalon[14]. In general, MGE-derived interneurons ultimately give rise to parvalbumin- and somatostatin-expressing cohorts, as well as most of the nitric oxide synthase (NOS)-expressing interneurons, whereas interneurons expressing calretinin, vasoactive intestinal peptide, reelin or cholecystokinin (CCK) and the remaining NOS-expressing interneurons arise from the CGE[14–17]. Thus, specific mouse reporter lines for MGE- and CGE-derived cells can be used to routinely target two nonoverlapping populations of interneurons throughout early postnatal development before the onset of subtype-defining molecular and electrophysiological characteristics. We examined the developmental profiles of excitatory synaptic inputs to MGE- and CGE-derived interneurons in the hippocampus, where *post hoc* morphological analyses of cell anatomy and stratification allow for further subdivision of these two broad interneuron classes. Our findings reveal stereotyped developmental differences between MGE- and CGE-derived interneurons with regards to their AMPAR- and NMDAR-mediated components of synaptic events driven by a common afferent pathway. Most notably, we identified a ganglionic eminence–dependent rule for a developmental switch in GluN2 subunit composition and

demonstrate that this switch can be acutely driven by repetitive activation of developing synapses.

RESULTS

Basic synaptic properties of MGE and CGE interneurons

To selectively target MGE-derived interneurons for synaptic analysis, we performed whole-cell voltage-clamp recordings from GFP^+ cells in acute hippocampal slices obtained from *Nkx2-1-cre:*RCE GFP transgenic mice (Fig. 1a), which specifically report MGE-derived neocortical and hippocampal interneurons[15]. To target CGE-derived interneurons, we used serotonin-3A receptor–GFP (*Htr3a-GFP*) reporter mice (Fig. 1b), as this receptor is an early and protracted marker for all CGE-derived neocortical interneurons[16,17]. To allow reliable comparison within a single afferent pathway common to both CGE- and MGE-derived interneurons, we focused on interneurons located within CA1 stratum radiatum and pyramidale and compared pharmacologically isolated excitatory synaptic events driven by Schaffer collateral stimulation (Fig. 1c–h). Pooled data across all developmental time points revealed significant differences in the rectification properties of AMPARs used by MGE- and CGE-derived interneurons (Fig. 1c,d,i). Current-voltage (*I–V*) relationships of AMPAR-mediated excitatory postsynaptic currents (EPSCs) in MGE-derived interneurons typically showed strong inward rectification, indicating that transmission in these cells is mediated by GluA2-lacking, calcium-permeable AMPARs (Fig. 1c,i)[18]. In contrast, transmission in CGE-derived cells is dominated by GluA2-containing, calcium-impermeable AMPARs, as evidenced by the relatively linear *I–V* relationships of AMPAR-mediated EPSCs in these cells (Fig. 1d,i). We pharmacologically confirmed this differential expression of calcium-permeable and calcium-impermeable AMPARs by MGE- and CGE-derived interneurons, respectively, in a subset of recordings with the calcium permeable AMPAR–selective antagonist philanthotoxin (Fig. 1e,f,j).

During the generation of *I–V* relationships in preliminary experiments in which both the AMPAR- and NMDAR-mediated components of transmission were intact, it became apparent that CGE-derived interneurons typically had larger NMDAR-mediated currents than their MGE-derived counterparts. Indeed, a comparison of NMDA-to-AMPA ratios between the two cell groups revealed a significantly larger contribution of NMDARs at Schaffer collateral CGE-derived cell synapses than that observed at Schaffer collateral inputs to MGE-derived interneurons (Fig. 1g,h,k). Despite this difference in the relative magnitude of NMDAR-mediated transmission, synaptic NMDARs in MGE- and CGE-derived interneurons showed no apparent differences in voltage dependence, with both yielding typical J-shaped *I–V* curves with negative slopes at holding potentials between −60 and −20 mV due to the voltage-dependent block by magnesium (Supplementary Fig. 1).

To determine whether the synaptic differences observed between MGE- and CGE-derived cells are maintained throughout development, we compared the synaptic profiles of cells recorded from neonate (postnatal day (P) 3 to P8) and juvenile (P14–P21) *Nkx2-1-cre:*RCE and *Htr3a-GFP* mice (Fig. 2). In addition to this developmental window, we also parsed the data on the basis of cell anatomy to ensure that our data sets would be generally applicable to MGE- and CGE-derived cells and would not be biased by one interneuron subtype in each

cohort. *Post hoc* morphological analysis of cells recorded within stratum radiatum of *Htr3a-GFP* mice generally revealed three anatomical profiles: (i) perisomatic-targeting basket cells (Fig. 2a); (ii) wide-range dendrite-targeting interneurons with axons covering the stratum radiatum, pyramidale and stratum oriens (Fig. 2b); and (iii) Schaffer collateral–associated interneurons with axons targeting the stratum radiatum (Fig. 2c). These anatomies are consistent with those of three subtypes of CGE-derived CCK-expressing interneurons[15,19,20], which validates the use of *Htr3a-GFP* reporter mice to target hippocampal CGE-derived interneurons. Consistent with our previous data set, Schaffer collateral inputs to all three CGE-derived cell types showed comparable AMPAR-mediated and pharmacologically isolated (by 6-nitro-2,3-dioxo-1,4-dihydroben zo[f]quinoxaline-7-sulfonamide (NBQX)) NMDAR-mediated EPSCs obtained at holding potentials of −60 and +40 mV, respectively, yielding NMDA-to-AMPA ratios close to unity (Fig. 2d,g,s). This ratio did not change through development from neonatal (Fig. 2d,s) to juvenile stages (Fig. 2g,s). Further analysis of AMPAR-mediated EPSCs, isolated pharmacologically by d(−)-2-amino-5-phosphonovaleric acid (AP5), revealed very modest inward rectification in the *I–V* relationships of Schaffer collateral CGE-derived interneuron synapses throughout development (Fig. 2e,f,h,i,t), indicating that the prevalence of edited GluA2 subunits in these cells is maintained from the earliest time points examined. Indeed, although the frequency of spontaneous EPSCs (sEPSCs) onto CGE-derived interneurons increased with maturation of the circuit, the kinetics and amplitudes of these unitary events remained constant through development for each CGE cell type (Supplementary Fig. 2).

Anatomically recovered GFP^+ cells recorded in *Nkx2-1-cre:*RCE mice typically resembled basket cells (Fig. 2j), bistratified cells (Fig. 2k) or ivy cells (Fig. 2l), which all derive from MGE progenitors[15]. In contrast to our observations in CGE-derived cells, Schaffer collateral MGE-derived interneuron synapses were dominated by AMPARs with significantly smaller NMDAR-to-AMPAR EPSC ratios throughout development (Fig. 2m,p,s). Moreover, all MGE-derived interneurons showed strongly inwardly rectifying AMPAR-mediated EPSCs, indicating prominent expression of GluA2-lacking calcium-permeable AMPARs at Schaffer collateral inputs (Fig. 2n,o,q,r,t). In agreement with this observation, sEPSCs in MGE-derived cells were larger and faster throughout development than those in CGE-derived cells, a finding that is consistent with the larger conductance and faster kinetics of calcium-permeable compared to calcium-impermeable AMPARs (Supplementary Fig. 2)[18]. Together these findings reveal striking differences between MGE- and CGE-derived interneurons with regards to their relative proportions of synaptic AMPARs and NMDARs, as well as their synaptic AMPAR subunit composition. However, there is a remarkable conservation of these basic synaptic properties within each subgroup throughout early postnatal development.

Developmental expression of GluN2 subunits

GluN2B-containing NMDARs have slower kinetics than GluN2A-containing receptors and are selectively blocked by ifenprodil and related compounds[21]. These biophysical and pharmacological differences enable the characterization of synaptic NMDAR GluN2 subunit composition (Fig. 3). At the neonatal stage, we found that pharmacologically isolated NMDAR EPSCs at Schaffer collateral inputs to both CGE- and MGE-derived interneurons

had slow kinetics and high ifenprodil sensitivity (Fig. 3a,c,e,f), indicating prominent expression of GluN2B-containing NMDARs at these synapses. At the juvenile stage, all MGE-derived cells, and the Schaffer collateral–associated cohort of CGE-derived cells, had NMDAR-mediated EPSCs with significantly faster decay kinetics and reduced ifenprodil sensitivity in comparison with the same cell types assayed in neonatal slices (Fig. 3b,e,f). These data indicate that a stereotyped developmental switch occurs from GluN2B- to GluN2A-containing NMDARs at Schaffer collateral inputs to all MGE-derived interneurons and also to the Schaffer collateral–associated subset of CGE-derived interneurons. In contrast, we found no significant developmental changes in the kinetics or ifenprodil sensitivity of NMDAR-mediated EPSCs in CGE-derived basket and dendrite-targeting cells (Fig. 3d–f), even when we extended our analysis into the adult stage (P40–P50; Supplementary Fig. 3), revealing that these interneurons maintain a high proportion of synaptic GluN2B-containing NMDARs throughout development.

Previous studies in principal cells found a correlation between post-synaptic NMDAR GluN2 subunit composition and presynaptic release probability during synapse maturation, in which GluN2B-containing NMDARs selectively expressed at immature synapses are driven by high–release probability inputs, whereas GluN2A-containing NMDARs localize to mature low–release probability synapses[22]. To probe for a similar correlation between release probability and NMDAR subunit composition during interneuron synapse maturation, we monitored NMDAR-mediated EPSC paired-pulse ratios (PPRs) as an indicator of release probability at different developmental stages. We did not detect a significant difference in PPRs between neonates and juveniles (Supplementary Fig. 4). Moreover, we did not detect any changes in NMDAR-mediated EPSC PPRs after ifenprodil-mediated depression of NMDARs (Supplementary Fig. 4). These data indicate that GluN2B- and GluN2A-containing NMDARs do not segregate between high– and low–release probability synapses in developing interneurons and additionally exclude the possibility of a confounding influence of Schaffer collateral presynaptic GluN2B-containing receptors on the interpretation of our findings with ifenprodil.

Similar properties at distinct afferent inputs

Differences in synaptic glutamate receptor subunit composition within the same cell at different synaptic inputs has been reported for both principal cells and interneurons[23–25]. This afferent specificity may occur in CA1 interneurons receiving inputs from both CA3 pyramidal cells (Schaffer collateral inputs) and CA1 pyramidal cells (alvear (ALV) inputs) such as MGE-derived basket and bistratified cells, which often have dendrites extending into both the stratum radiatum and oriens. Thus, to probe for any potential afferent pathway specificity in the developmental program of MGE-derived interneuron synapse maturation, we performed dual pathway stimulation experiments in individual MGE-derived interneurons at the neonatal and juvenile stages to simultaneously monitor Schaffer collateral and ALV inputs within the same cell. At both the individual-cell and population levels, we found that Schaffer collateral–driven and ALV-driven synapses showed similar inwardly rectifying AMPAR-mediated synaptic currents (Fig. 4a), as well as equivalent proportions of NMDARs and AMPARs throughout development (Fig. 4b). Moreover, synapses in both input pathways showed a progressive speeding in NMDAR kinetics

coincident with a reduction in ifenprodil sensitivity, but the ALV inputs lagged behind the developmental trajectory of the Schaffer collateral synapses (Fig. 4c–f). In general, these findings indicate that excitatory synapses onto hippocampal MGE-derived basket and bistratified cells undergo a stereotyped developmental program at both Schaffer collateral and ALV inputs, but the time course of this process has afferent specificity. In contrast, the synaptic properties of ALV inputs to radiatum-dwelling CGE-derived basket cells, the only subset of CGE cells we regularly found to extend dendrites into the oriens throughout development, remained constant with age, which is similar to our observations for Schaffer collateral inputs to these cells (Supplementary Fig. 5).

To examine whether GluN2B-containing NMDARs influence excitation spike (E-S) coupling in young MGE-derived interneurons, we probed the effects of ifenprodil on action-potential firing elicited by repetitive afferent stimulation (Fig. 5). To minimize the potential confounding influence of polysynaptic activity, we performed most of our experiments using ALV inputs; however, a smaller subset of recordings using Schaffer collateral inputs yielded similar results, so we pooled the data. In cell-attached recordings from young (P6–P9) MGE-derived cells, ifenprodil reliably decreased spike jitter on the first event of a brief train consisting of three stimuli delivered at 40 Hz (Fig. 5a–c,e). Moreover, ifenprodil also significantly reduced the probability of observing a spike on the second and third pulses of the train in these recordings from young cells (Fig. 5a,b,f,h). Together these findings confirm that the slower kinetics of GluN2B-containing NMDARs influence the synaptic integration properties of young MGE-derived interneurons to regulate both the summation and timing of action-potential generation. In contrast, ifenprodil did not alter either spike jitter or probability in P18–P21 MGE-derived interneurons, which is consistent with the observed developmental reduction in synaptic participation of GluN2B-containing NMDARs (Fig. 5d,e,g,h).

Activity-dependent changes in GluN2 subunits

In the intact nervous system, sensory experience drives circuit development, including synaptic refinement, as an animal interacts with its environment during postnatal development. For example, in primary visual and barrel cortices, sensory experience of the appropriate modality induces the GluN2B-to-GluN2A subunit switch at synapses between cortical principal cells[10,26,27]. A similar switch in neonatal hippocampal pyramidal cell NMDAR subunit composition can be rapidly induced by repetitive synaptic activation *in vitro*[6]. Because our data indicate that MGE-derived hippocampal interneurons undergo a developmental switch in synaptic NMDAR subunit composition similar to that observed in pyramidal cells, we tested whether Schaffer collateral inputs onto MGE-derived interneurons show rapid use-dependent plasticity of synaptic NMDAR GluN2 subunit composition (Fig. 6). Immediately after establishing the whole-cell configuration and finding a Schaffer collateral input, we subjected synapses to an induction protocol (2 Hz afferent stimulation for 1.5 min) analogous to that driving NMDAR plasticity in pyramidal cells[6] but with cells voltage clamped at −70 mV to promote calcium influx through calcium-permeable AMPARs, which is crucial for several forms of interneuron plasticity[28,29]. After induction, we probed pharmacologically isolated NMDAR-mediated transmission at a holding potential of +40 mV and obtained kinetic and ifenprodil sensitivity profiles to

compare with cells that we did not subject to the induction protocol. NMDAR EPSCs in neonatal MGE-derived cells subjected to the induction protocol were significantly faster and less sensitive to ifenprodil when compared with cells that we did not subject to the induction protocol (Fig. 6a–c,g,h). In contrast, the same induction protocol did not alter NMDAR kinetics or ifenprodil sensitivity in neonatal CGE-derived interneurons even when we paired the induction protocol with cell depolarization at 0 mV to promote calcium influx through NMDARs (Supplementary Fig. 6). These findings indicate that repetitive synaptic activation can acutely drive a GluN2B-to-GluN2A subunit switch in synaptic NMDARs expressed by MGE- but not CGE-derived interneurons, revealing a new form of interneuron plasticity that recapitulates normal development on a rapid timescale. Notably, the ability to evoke activity-induced changes in NMDAR EPSC kinetics and ifenprodil sensitivity paralleled the developmental profile of GluN2B expression in MGE-derived interneurons, which is consistent with a developmental occlusion of plasticity by the natural loss of synaptic GluN2B subunit–containing NMDARs in these cells (Fig. 6g,h).

Activity-driven NMDAR plasticity at immature pyramidal cell synapses requires a rise in postsynaptic calcium influx through NMDARs along with activation of mGluR5 (ref. 8). Inclusion of the calcium chelator BAPTA in the recording electrode prevented MGE-derived interneuron NMDAR plasticity, revealing a similar requirement for increased amounts of postsynaptic calcium (Fig. 6e,i,j). However, in contrast to the results from pyramidal cells, the activity-driven switch in MGE-derived interneuron GluN2 subunit composition proceeds independently of NMDAR or mGluR5 activation, as antagonism of these receptors with AP5 or 3-((2-methyl-4-thiazolyl)ethynyl)pyridine (MTEP), respectively, did not prevent changes in NMDAR kinetics or ifenprodil sensitivity in cells subjected to the induction protocol (Fig. 6d,i,j). Instead, our findings implicate calcium influx through calcium-permeable AMPARs as the probable trigger, as blockade of AMPARs with NBQX during induction prevented activity-driven changes in MGE-derived interneuron NMDARs (Fig. 6f,i,j). Despite the presence of GluN2B-containing NMDARs and calcium-permeable AMPARs at ALV inputs to neonatal MGE-derived interneurons, the induction protocol did not alter the kinetics or ifenprodil sensitivity of NMDARs at these synapses (Supplementary Fig. 7). Thus, although MGE-derived interneurons show similar developmental programs for NMDAR subunit composition at both Schaffer collateral and ALV inputs, acutely driven plasticity of NMDARs in neonatal MGE-derived interneurons is specific to the Schaffer collateral pathway. To determine whether NMDAR plasticity is input specific within the Schaffer collateral pathway (that is, homosynaptic), we simultaneously monitored two sets of Schaffer collateral inputs onto P8–P10 MGE interneurons but conditioned only one path (test) and left the second path (naive) unstimulated during conditioning of the test path. After induction, the kinetics and ifenprodil sensitivity of the test and naive paths were indistinguishable (test path, 216 ± 11 ms, 56% ± 6% of control value before drug treatment; naive path, 212 ± 11 ms, 56% ± 5% of control; $n = 9$ cells recorded in nine slices from three mice; values are mean ± s.e.m.), indicating that the activity-driven loss of GluN2B is not input specific within the Schaffer collateral path. Though inconsistent with observations in young pyramidal cells, where activity-driven loss of GluN2B is homosynaptic[6], the observed heterosynaptic spread of NMDAR plasticity in young MGE-derived interneurons

is reminiscent of a form of long-term depression reported in unidentified hippocampal interneurons that distributes across multiple inputs after conditioning of only one path[30].

During the second and third postnatal weeks, CA3 pyramidal cell populations show synchronized action-potential burst firing that is capable of driving synaptic plasticity at excitatory synapses between principal cells within the hippocampal network[31–33]. The conspicuous overlap in developmental windows for the emergence of CA3 network burst firing and MGE-derived interneuron NMDAR plasticity prompted us to conduct a final series of experiments to examine whether such intrinsic network-driven activity could promote the GluN2B-to-GluN2A subunit switch at nascent MGE-derived basket and bistratified cell synapses. In the absence of any synaptic inhibitors, treatment of intact P6–P8 transverse hippocampal slices containing both CA3 and CA1 with a modified artificial cerebrospinal fluid (ACSF) (5 mM K^+, 1.5 mM Ca^{2+} and 1 mM Mg^{2+}) that more closely resembles the extracellular ionic conditions in the developing brain[34] consistently produced rhythmic burst firing in CA3 pyramidal cells (Fig. 7a,b). After 5–8 min of recording CA3 pyramidal-cell burst firing in modified ACSF, we returned the slices to normal ACSF and targeted CA1 MGE-derived basket and bistratified interneurons for recordings of pharmacologically isolated NMDAR-mediated EPSCs driven by Schaffer collateral stimulation. We found that NMDAR-mediated events in MGE-derived cells from treated slices had reduced decay times and ifenprodil sensitivity as compared to the same cell types in naive slices (Fig. 7c–f). Notably, treatment with modified ACSF did not generally alter NMDARs, as burst firing did not alter NMDAR ifenprodil sensitivity or kinetics at ALV inputs onto neonatal MGE-derived cells or Schaffer collateral CGE-derived interneuron synapses (Supplementary Figs. 6 and 7). Thus, recurrent network activity is able to drive the GluN2B-to-GluN2A subunit switch in synaptic NMDARs expressed at immature Schaffer collateral MGE-derived interneuron synapses, potentially implicating the emergence of intrinsic CA3 network burst-firing activity as a physiologically relevant trigger for refining these synapses during early postnatal development.

DISCUSSION

The integration of a given neuron into a circuit is dependent on the establishment and refinement of excitatory synaptic inputs onto that cell for efficient network recruitment. Here we found that transmission at Schaffer collateral MGE-derived interneuron synapses is dominated by calcium-permeable AMPARs in both neonates and juveniles, with only a minor contribution of NMDARs (NMDA-to-AMPA ratio of ~0.25) in these cells at both time points. In contrast Schaffer collateral CGE-derived interneuron synapses express calcium-impermeable AMPARs and have large NMDAR-mediated components (NMDA-to-AMPA ratios of ~1) throughout development. At the neonatal stage, GluN2B-containing NMDARs carried a large proportion (>70%) of the NMDAR-mediated EPSCs in both MGE- and CGE-derived interneurons, and this large contribution of GluN2B-containing receptors persisted in most juvenile CGE-derived interneurons. However, the relative contribution of GluN2Bcontaining receptors was markedly reduced in all juvenile MGE-derived cells and in the Schaffer collateral–associated subset of CGE cells. A similar switch in NMDAR subunit composition could be acutely driven in neonatal MGE- but not CGE-

derived cells, revealing a new activity-dependent form of synaptic plasticity that is available to developing excitatory synaptic inputs onto MGE-derived cells.

Nascent glutamatergic contacts between principal cells undergo a stereotyped developmental program, with transmission shifting from being predominantly NMDAR mediated to AMPAR mediated during the first few postnatal weeks[35–37]. Indeed, morphological and electrophysiological studies have revealed an abundance of silent synapses containing only NMDARs at immature synapses between principal cells throughout the neonatal nervous system (reviewed in ref. 38). In contrast, all interneuron subtypes examined showed prominent AMPAR-mediated components to the excitatory synaptic drive at neonatal stages and stability in the relative contribution of synaptic AMPARs and NMDARs throughout development. However, MGE- and CGE-derived interneurons differed greatly in the relative proportion of synaptic transmission carried by AMPARs and NMDARs, as well as the calcium permeability of their AMPARs. CGE-derived cells expressed large NMDA EPSCs and calcium-impermeable AMPARs, whereas MGE-derived cells expressed relatively small NMDA EPSCs and calcium-permeable AMPARs. These observations provide some order to the seemingly random expression of calcium-permeable and calcium-impermeable AMPARs by unidentified hippocampal interneurons[39–43]. However, an absolute origin-dependent rule for the expression of calcium-permeable compared to calcium-impermeable AMPARs is probably too simplistic, as individual interneurons have been demonstrated to target calcium-permeable and calcium-impermeable AMPARs to synapses innervated by distinct afferent inputs[25,44]. Notably, distinct forms of synaptic plasticity in divergent CA1 interneurons have been attributed to the expression of calcium-permeable and calcium-impermeable AMPARs (reviewed in ref. 45). Consistent with our data, calcium permeable AMPAR–dependent forms of plasticity have been reported in bistratified, ivy, oriens lacunosum molecular (OLM) and parvalbumin-expressing basket, cells[29,46,47], all of which are MGE derived[15].

One feature common to principal cells and all interneurons that we examined is the prominent expression of GluN2B-containing synaptic NMDARs at neonatal stages, suggesting an important role for these receptors in the circuit integration of both excitatory and inhibitory elements of developing networks. The slow kinetics of these receptors may be necessary to prolong the synaptic integration window of young neurons for effective recruitment in immature networks. Indeed, we found that GluN2B-containing NMDARs promote spike generation during repetitive synaptic stimulation of young MGE-derived cells. In most CGE-derived interneurons, these ifenprodil-sensitive NMDARs are retained into the adult stage. However, MGE-derived interneurons and the Schaffer collateral–associated subset of CGE-derived interneurons undergo a developmental shift and replace these ‘immature’ NMDARs with ‘mature’ GluN2A subunit–dominated NMDARs. In this respect, Schaffer collateral–associated and MGE-derived interneuron synapses are similar to those between principal cells, which also show a maturational GuN2B-to-GuN2A subunit switch[5–10]. Notably, the timing of this switch to the kinetically faster GluN2A-dominated NMDARs parallels a number of developmental changes within parvalbumin expressing basket cells, including decreases in membrane time constant and action-potential duration, that promote their progression from slow to fast inhibitory signaling devices[48]. Our current

findings indicate that MGE-derived bistratified and ivy cells may undergo a similar developmental program to endow the circuit with temporally precise dendritic inhibition.

Acute sensory experience or synaptic activity can rapidly drive the GluN2B-to-GluN2A subunit switch in neonatal pyramidal cells of the visual cortex and hippocampus, respectively[6,10,26]. We found that MGE-derived interneurons undergo a similar rapid activity-dependent switch in GluN2 subunit composition. Notably, the GluN2B-to-GluN2A switch is dependent on a rise in the amount of intracellular calcium in both principal cells and interneurons. However, whereas principal cells rely on NMDAR activation as the source of calcium, MGE-derived interneurons utilize calcium-permeable AMPARs. Indeed although calcium impermeable AMPAR–expressing Schaffer collateral–associated cells also undergo a developmental GluN2B-to-GluN2A switch, these cells did not show acute plasticity of NMDARs, which is consistent with a requirement of calcium-permeable AMPARs in driving this form of plasticity in interneurons. Calcium influx through calcium-permeable AMPARs has been implicated in diverse forms of synaptic plasticity, including both long-term depression and long-term potentiation in juvenile hippocampal interneurons[24,46]. Thus, like pyramidal cells[6], activity patterns that evoke plasticity in phenotypically mature interneurons are used by immature synapses to evoke a rapid switch in the GluN2 subunits of neonatal interneurons.

In conclusion, we investigated the developmental expression patterns of glutamatergic receptors used at Schaffer collateral inputs to CA1 hippocampal interneurons. Our findings provide new insight into the distinct developmental programs for synaptic maturation in MGE- and CGE-derived interneurons and may relate to observations that early, but not late, postnatal disruption of excitatory synaptic input to specific interneuron cohorts can precipitate neurological disorders such as schizophrenia[49].

ONLINE METHODS

Electrophysiology

Both males and females from the *Nkx2-1-cre:*RCE (Swiss Webster background) and *Htr3a-GFP* (C57Bl/6J background) reporter lines were used throughout the study. Mice were anesthetized with isoflurane and then decapitated in accordance with US National Institutes of Health animal care and use guidelines. Transverse hippocampal slices (300-μm thick) were cut in ice-cold high-sucrose ACSF containing (in mM): 87 NaCl, 2.5 KCl, 0.5 $CaCl_2$, 7 $MgSO_4$, 1.25 NaH_2PO_4, 25 $NaHCO_3$, 25 glucose and 75 sucrose equilibrated with 95% O_2 and 5% CO_2. Slices were then placed at 35 °C for 30 min and allowed to recover for at least 1 h in ACSF at room temperature. The ACSF used for electrophysiological recordings contained (in mM): 119 NaCl, 2.5 KCl, 2.5 $CaCl_2$, 1.3 $MgSO_4$, 1 NaH_2PO_4, 26.2 $NaHCO_3$ and 11 glucose equilibrated with 95% O_2 and 5% CO_2. For Figure 6, in which the extracellular potassium concentration was elevated (K^+ solution), the ACSF composition was identical except for (in mM): 5 KCl, 1.5 $CaCl_2$ and 1 $MgSO_4$. Whole-cell patch clamp recordings were made from visually identified GFP-expressing neurons. The whole-cell solution contained (in mM): 135 cesium methanesulfonate, 8 KCl, 10 HEPES, 4 Mg-ATP, 0.4 Na-GTP, 5 QX-314, 0.1 spermine, 0.5 EGTA and 2 mg ml^{-1} biocytin (Sigma-Aldrich) (pH 7.3).

EPSCs were evoked by electrical stimulation of Schaffer collateral and/or alvear axons using monopolar stimulating electrodes placed in the stratum radiatum of CA1 or the alveus (0.1–0.2 Hz stimulation frequency). Isolated AMPA EPSCs for *I–V* curves were done in presence of 100 μM AP5 and 50 μM picrotoxin. To derive the rectification index, AMPA EPSC peak amplitudes at negative potentials were fit with a linear function, and the rectification index was calculated as the ratio of the measured AMPA EPSC at +40 mV divided by the value predicted by extrapolating the linear fit to +40 mV. NMDA EPSCs were obtained in the presence of NBQX (5 μM) and picrotoxin (50 μM), and cells were voltage clamped at +40 mV. NMDA EPSC decay was fit with a double exponential function using OriginLab software (Northampton, MA), and decay kinetics are expressed as a weighted decay-time constant. All receptor antagonists were bath applied at least 15 min before and during the induction protocol. The induction protocol for the activity-dependent switch in GluN2 subunits was 180 stimulations of Schaffer collaterals (or the alveus) at 2 Hz, which started within 3 min of obtaining the whole-cell configuration to avoid 'wash-out'. The holding potential was −70 mV during induction unless otherwise indicated. All drugs except for picrotoxin (Sigma Aldrich) were obtained from Tocris Cookson. Recordings in which the access resistance changed by more than 10% were discarded and were not included in the analysis. Recordings were performed using a Multiclamp 700B patch-clamp amplifier (Axon Instruments, Foster City, CA); signals were filtered at 4 kHz, digitized at 10 kHz and displayed and analyzed online using pClamp 9.2 (Axon Instruments). sEPSC data were analyzed using ClampFit 10 (Axon Instruments). sEPSCs were automatically detected using template matching, and time constants were calculated using a fit of the averaged trace. A minimum of 40 events were used for each cell.

For E-S coupling experiments, recordings were made from either neonate or juvenile CA1 hippocampal MGE-derived interneurons in the cell-attached configuration using pipettes filled with oxygenated ACSF. Forty-hertz trains of three stimuli were evoked every 10 s with monopolar stimulating electrodes placed in either the stratum radiatum of CA1 or the alveus. Each experiment consisted of a 5-min baseline period (30 sweeps) followed by 15 min in the presence of 5 μM ifenprodil (90 sweeps) and a final 5 min period in the presence of 5 μM ifenprodil and 10 μM DNQX. In all cases, the addition of DNQX abolished the evoked spikes, confirming that the spikes were synaptically driven. To minimize any potential confounding influence of polysynaptic activity on E-S coupling, only spikes that occurred within 10 ms of each respective stimulus within the 40-Hz train were included in the analyses. The spike jitter analysis was limited to spikes evoked by the first stimulus of the 40-Hz trains to avoid influences of summation, and jitter was calculated as the s.d. in the latency of the spike peak. To determine the effects of ifenprodil on spike probability during summation, the combined number of spikes evoked by the second and third stimuli of the trains were analyzed. For each experiment, the spike jitter and probability of spiking were calculated for the last 20 sweeps of the baseline and ifenprodil epochs.

Slices containing biocytin-filled cells were drop fixed in 4% paraformaldehyde overnight at 4 °C and then permeabilized (freeze thaw or Triton) and incubated with Alexa 555–conjugated avidin (Molecular Probes). After multiple washes, the slices were resectioned (70 μm) on a freezing microtome (Microm) and mounted on gelatin-coated slides using

Mowiol (Calbiochem) mounting medium. Stacked *Z*-section images of recorded cells revealed by biocytin conjugation were obtained with a Leica TCS SP2 RS confocal microscope. Frames of the maximum projection images for each cell were stitched together, converted to grayscale and inverted in Adobe Photoshop. In some cases, two-dimensional reconstructions were traced from stacked *Z*-section images using Neurolucida (MicroBrightField, Williston, VT).

Statistics

Values are presented as the mean ± s.e.m. Unless otherwise indicated, statistical significance was tested using parametric paired or Student's *t* tests, as appropriate. No statistical methods were used to predetermine sample sizes; however, our sample sizes conformed to those generally used in similar studies. For all data sets compared using parametric tests, the data were assumed to be normally distributed, but this was not formally tested.

Supplementary Material

Refer to Web version on PubMed Central for supplementary material.

Acknowledgments

D. Abebe and X. Yuan provided expert technical assistance. We thank S. Anderson (University of Pennsylvania) for providing the *Nkx2-1-cre* driver line and G. Fishell (New York University) for providing the RCE reporter line. This work was supported by a Eunice Kennedy-Shriver National Institute of Child Health and Human Development intramural award to C.J.M. and a PRAT Fellowship to J.A.M.

References

1. Isaac JT. Postsynaptic silent synapses: evidence and mechanisms. Neuropharmacology. 2003; 45:450–460. [PubMed: 12907306]
2. Pickard L, et al. Transient synaptic activation of NMDA receptors leads to the insertion of native AMPA receptors at hippocampal neuronal plasma membranes. Neuropharmacology. 2001; 41:700–713. [PubMed: 11640924]
3. Eybalin M, Caicedo A, Renard N, Ruel J, Puel JL. Transient Ca^{2+}-permeable AMPA receptors in postnatal rat primary auditory neurons. Eur. J. Neurosci. 2004; 20:2981–2989. [PubMed: 15579152]
4. Kumar SS, Bacci A, Kharazia V, Huguenard JR. A developmental switch of AMPA receptor subunits in neocortical pyramidal neurons. J. Neurosci. 2002; 22:3005–3015. [PubMed: 11943803]
5. Sheng M, Cummings J, Roldan LA, Jan YN, Jan LY. Changing subunit composition of heteromeric NMDA receptors during development of rat cortex. Nature. 1994; 368:144–147. [PubMed: 8139656]
6. Bellone C, Nicoll RA. Rapid bidirectional switching of synaptic NMDA receptors. Neuron. 2007; 55:779–785. [PubMed: 17785184]
7. Bellone C, Mameli M, Luscher C. *In utero* exposure to cocaine delays postnatal synaptic maturation of glutamatergic transmission in the VTA. Nat. Neurosci. 2011; 14:1439–1446. [PubMed: 21964489]
8. Matta JA, Ashby MC, Sanz-Clemente A, Roche KW, Isaac JT. mGluR5 and NMDA receptors drive the experience- and activity-dependent NMDA receptor NR2B to NR2A subunit switch. Neuron. 2011; 70:339–351. [PubMed: 21521618]
9. Sanz-Clemente A, Matta JA, Isaac JT, Roche KW. Casein kinase 2 regulates the NR2 subunit composition of synaptic NMDA receptors. Neuron. 2010; 67:984–996. [PubMed: 20869595]

10. Quinlan EM, Philpot BD, Huganir RL, Bear MF. Rapid, experience-dependent expression of synaptic NMDA receptors in visual cortex *in vivo*. Nat. Neurosci. 1999; 2:352–357. [PubMed: 10204542]
11. Somogyi P, Klausberger T. Defined types of cortical interneurone structure space and spike timing in the hippocampus. J. Physiol. (Lond.). 2005; 562:9–26. [PubMed: 15539390]
12. Korotkova T, Fuchs EC, Ponomarenko A, von Engelhardt J, Monyer H. NMDA receptor ablation on parvalbumin-positive interneurons impairs hippocampal synchrony, spatial representations, and working memory. Neuron. 2010; 68:557–569. [PubMed: 21040854]
13. Fuchs EC, et al. Recruitment of parvalbumin-positive interneurons determines hippocampal function and associated behavior. Neuron. 2007; 53:591–604. [PubMed: 17296559]
14. Wonders CP, Anderson SA. The origin and specification of cortical interneurons. Nat. Rev. Neurosci. 2006; 7:687–696. [PubMed: 16883309]
15. Tricoire L, et al. A blueprint for the spatiotemporal origins of mouse hippocampal interneuron diversity. J. Neurosci. 2011; 31:10948–10970. [PubMed: 21795545]
16. Vucurovic K, et al. Serotonin 3A receptor subtype as an early and protracted marker of cortical interneuron subpopulations. Cereb. Cortex. 2010; 20:2333–2347. [PubMed: 20083553]
17. Lee S, Hjerling-Leffler J, Zagha E, Fishell G, Rudy B. The largest group of superficial neocortical GABAergic interneurons expresses ionotropic serotonin receptors. J. Neurosci. 2010; 30:16796–16808. [PubMed: 21159951]
18. Traynelis SF, et al. Glutamate receptor ion channels: structure, regulation, and function. Pharmacol. Rev. 2010; 62:405–496. [PubMed: 20716669]
19. Daw MI, Tricoire L, Erdelyi F, Szabo G, McBain CJ. Asynchronous transmitter release from cholecystokinin-containing inhibitory interneurons is widespread and target-cell independent. J. Neurosci. 2009; 29:11112–11122. [PubMed: 19741117]
20. Morozov YM, Torii M, Rakic P. Origin, early commitment, migratory routes, and destination of cannabinoid type 1 receptor-containing interneurons. Cereb. Cortex. 2009; 19(suppl. 1):78–89.
21. Williams K, Russell SL, Shen YM, Molinoff PB. Developmental switch in the expression of NMDA receptors occurs *in vivo* and *in vitro*. Neuron. 1993; 10:267–278. [PubMed: 8439412]
22. Chavis P, Westbrook G. Integrins mediate functional pre- and postsynaptic maturation at a hippocampal synapse. Nature. 2001; 411:317–321. [PubMed: 11357135]
23. Ito I, Kawakami R, Sakimura K, Mishina M, Sugiyama H. Input-specific targeting of NMDA receptor subtypes at mouse hippocampal CA3 pyramidal neuron synapses. Neuropharmacology. 2000; 39:943–951. [PubMed: 10727704]
24. Lei S, McBain CJ. Distinct NMDA receptors provide differential modes of transmission at mossy fiber-interneuron synapses. Neuron. 2002; 33:921–933. [PubMed: 11906698]
25. Tóth K, McBain CJ. Afferent-specific innervation of two distinct AMPA receptor subtypes on single hippocampal interneurons. Nat. Neurosci. 1998; 1:572–578. [PubMed: 10196564]
26. Philpot BD, Sekhar AK, Shouval HZ, Bear MF. Visual experience and deprivation bidirectionally modify the composition and function of NMDA receptors in visual cortex. Neuron. 2001; 29:157–169. [PubMed: 11182088]
27. Mierau SB, Meredith RM, Upton AL, Paulsen O. Dissociation of experience-dependent and -independent changes in excitatory synaptic transmission during development of barrel cortex. Proc. Natl. Acad. Sci. USA. 2004; 101:15518–15523. [PubMed: 15492224]
28. Mahanty NK, Sah P. Calcium-permeable AMPA receptors mediate long-term potentiation in interneurons in the amygdala. Nature. 1998; 394:683–687. [PubMed: 9716132]
29. Oren I, Nissen W, Kullmann DM, Somogyi P, Lamsa KP. Role of ionotropic glutamate receptors in long-term potentiation in rat hippocampal CA1 oriens-lacunosum moleculare interneurons. J. Neurosci. 2009; 29:939–950. [PubMed: 19176803]
30. McMahon LL, Kauer JA. Hippocampal interneurons express a novel form of synaptic plasticity. Neuron. 1997; 18:295–305. [PubMed: 9052799]
31. Miles R, Wong RK. Single neurones can initiate synchronized population discharge in the hippocampus. Nature. 1983; 306:371–373. [PubMed: 6316152]

32. Stoop R, Conquet F, Zuber B, Voronin LL, Pralong E. Activation of metabotropic glutamate 5 and NMDA receptors underlies the induction of persistent bursting and associated long-lasting changes in CA3 recurrent connections. J. Neurosci. 2003; 23:5634–5644. [PubMed: 12843266]
33. Ho MT, et al. Burst firing induces postsynaptic LTD at developing mossy fibre-CA3 pyramid synapses. J. Physiol. (Lond.). 2009; 587:4441–4454. erratum **587**, 5798 (2009). [PubMed: 19635819]
34. Sanchez-Vives MV, McCormick DA. Cellular and network mechanisms of rhythmic recurrent activity in neocortex. Nat. Neurosci. 2000; 3:1027–1034. [PubMed: 11017176]
35. Durand GM, Kovalchuk Y, Konnerth A. Long-term potentiation and functional synapse induction in developing hippocampus. Nature. 1996; 381:71–75. [PubMed: 8609991]
36. Zhang L, Warren RA. Postnatal development of excitatory postsynaptic currents in nucleus accumbens medium spiny neurons. Neuroscience. 2008; 154:1440–1449. [PubMed: 18554817]
37. Isaac JT, Crair MC, Nicoll RA, Malenka RC. Silent synapses during development of thalamocortical inputs. Neuron. 1997; 18:269–280. [PubMed: 9052797]
38. Kerchner GA, Nicoll RA. Silent synapses and the emergence of a postsynaptic mechanism for LTP. Nat. Rev. Neurosci. 2008; 9:813–825. [PubMed: 18854855]
39. McBain CJ, Dingledine R. Heterogeneity of synaptic glutamate receptors on CA3 stratum radiatum interneurones of rat hippocampus. J. Physiol. (Lond.). 1993; 462:373–392. [PubMed: 8101227]
40. Morin F, Beaulieu C, Lacaille JC. Membrane properties and synaptic currents evoked in CA1 interneuron subtypes in rat hippocampal slices. J. Neurophysiol. 1996; 76:1–16. [PubMed: 8836204]
41. Petralia RS, Wang YX, Mayat E, Wenthold RJ. Glutamate receptor subunit 2-selective antibody shows a differential distribution of calcium-impermeable AMPA receptors among populations of neurons. J. Comp. Neurol. 1997; 385:456–476. [PubMed: 9300771]
42. Catania MV, et al. AMPA receptor subunits are differentially expressed in parvalbumin- and calretinin-positive neurons of the rat hippocampus. Eur. J. Neurosci. 1998; 10:3479–3490. [PubMed: 9824461]
43. Tóth K, McBain CJ. Target-specific expression of pre- and postsynaptic mechanisms. J. Physiol. (Lond.). 2000; 525:41–51. [PubMed: 10811723]
44. Topolnik L, Congar P, Lacaille JC. Differential regulation of metabotropic glutamate receptor- and AMPA receptor-mediated dendritic Ca^{2+} signals by presynaptic and postsynaptic activity in hippocampal interneurons. J. Neurosci. 2005; 25:990–1001. [PubMed: 15673681]
45. Kullmann DM, Lamsa KP. Long-term synaptic plasticity in hippocampal interneurons. Nat. Rev. Neurosci. 2007; 8:687–699. [PubMed: 17704811]
46. Szabo A, et al. Calcium-permeable AMPA receptors provide a common mechanism for LTP in glutamatergic synapses of distinct hippocampal interneuron types. J. Neurosci. 2012; 32:6511–6516. [PubMed: 22573673]
47. Nissen W, Szabo A, Somogyi J, Somogyi P, Lamsa KP. Cell type-specific long-term plasticity at glutamatergic synapses onto hippocampal interneurons expressing either parvalbumin or CB1 cannabinoid receptor. J. Neurosci. 2010; 30:1337–1347. [PubMed: 20107060]
48. Doischer D, et al. Postnatal differentiation of basket cells from slow to fast signaling devices. J. Neurosci. 2008; 28:12956–12968. [PubMed: 19036989]
49. Belforte JE, et al. Postnatal NMDA receptor ablation in corticolimbic interneurons confers schizophrenia-like phenotypes. Nat. Neurosci. 2010; 13:76–83. [PubMed: 19915563]

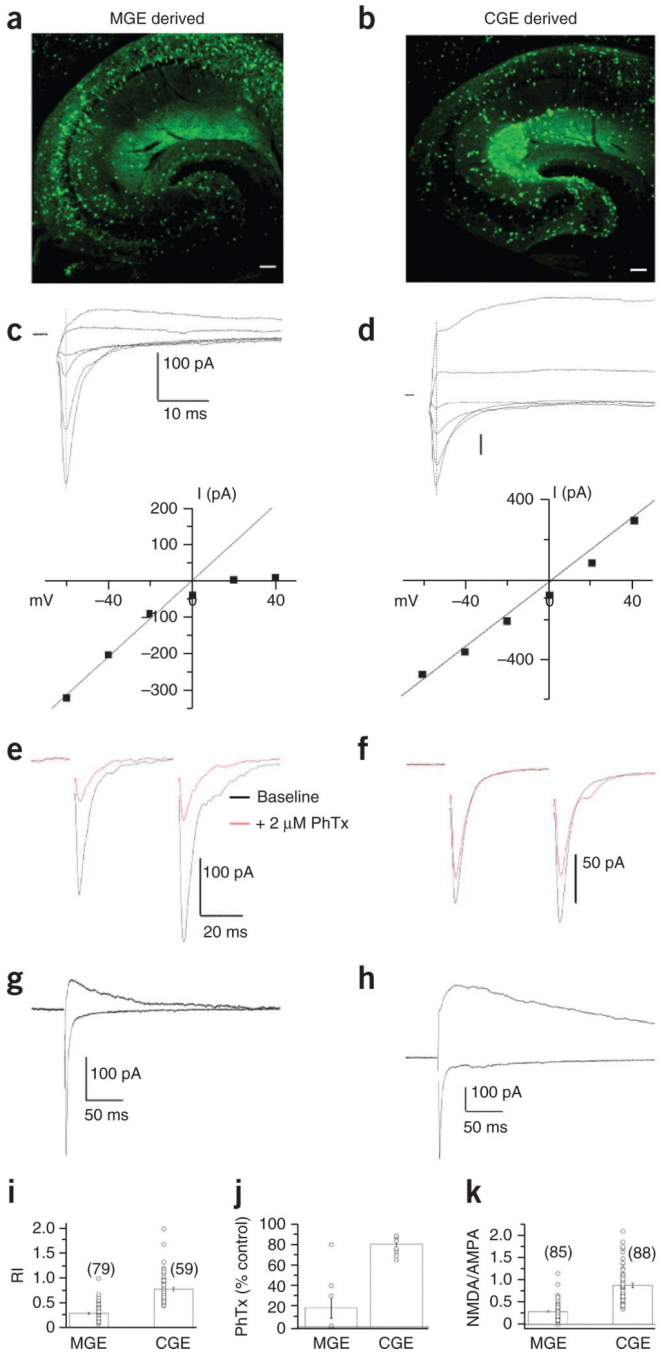

Figure 1. MGE- and CGE-dependent expression of synaptic glutamate receptors

(**a,b**) MGE- and CGE-derived cohorts of inhibitory interneurons were targeted using hippocampal slices derived from the *Nkx2-1-cre:*RCE GFP and *Htr3a-GFP* reporter mouse lines, respectively. Scale bars, 100 μm). (**c,d**) Top, representative total glutamate receptor (AMPAR and NMDAR)-mediated EPSCs evoked between −60 mV and +40 mV in 20-mV increments triggered by Schaffer collateral stimulation in MGE-derived (**c**) and CGE-derived (**d**) interneurons located in CA1 stratum radiatum. Bottom, *I–V* relationships of the AMPAR-mediated component measured at the time point of the EPSC peak obtained at −60

mV (indicated by dotted lines). Lines are the extrapolated linear fit of the data between −60 mV and 0 mV to reveal deviations from linearity at positive potentials. (**e,f**) AMPAR-mediated EPSCs before (black) and after (red) application of 2 μM philanthotoxin (PhTx) for representative recordings from MGE-derived (**e**) and CGE-derived (**f**) interneurons. EPSCs were evoked as pairs (with a 50-ms interstimulus interval), and PhTx did not alter the PPRs. (**g,h**) Representative EPSC traces from an MGE-derived (**g**) and CGE-derived (**h**) interneuron measured at −60 mV and +40 mV to extract the NMDAR-to-AMPAR amplitude ratio. (**i**–**k**) Summary plots of the AMPAR rectification index (RI) (**i**; MGE, 79 cells from 79 slices from 57 mice; CGE, 59 cells from 59 slices from 51 mice), philanthotoxin sensitivity (**j**; MGE, 8 cells from 8 slices from 5 mice; CGE, 8 cells from 8 slices from 6 mice) and NMDAR-to-AMPAR ratios (**k**; MGE, 85 cells from 85 slices from 57 mice; CGE, 88 cells from 88 slices from 51 mice) measured from all MGE- and CGE-derived interneurons regardless of their developmental age or anatomical identity. MGE-derived interneurons typically had AMPARs with significantly lower rectification indices ($P = 2.73 \times 10^{-25}$, degrees of freedom (d.f.) = 136, $t = -12.9$), higher philanthotoxin sensitivity ($P = 7.9 \times 10^{-5}$, d.f. = 14, $t = -5.5$) and lower NMDA-to-AMPA ratios ($P = 1.87 \times 10^{-20}$, d.f. = 171, $t = -10.6$) than their CGE-derived counterparts (P values were determined by unpaired t tests). Group data are presented as mean ± s.e.m., with results from individual experiments represented by open circles.

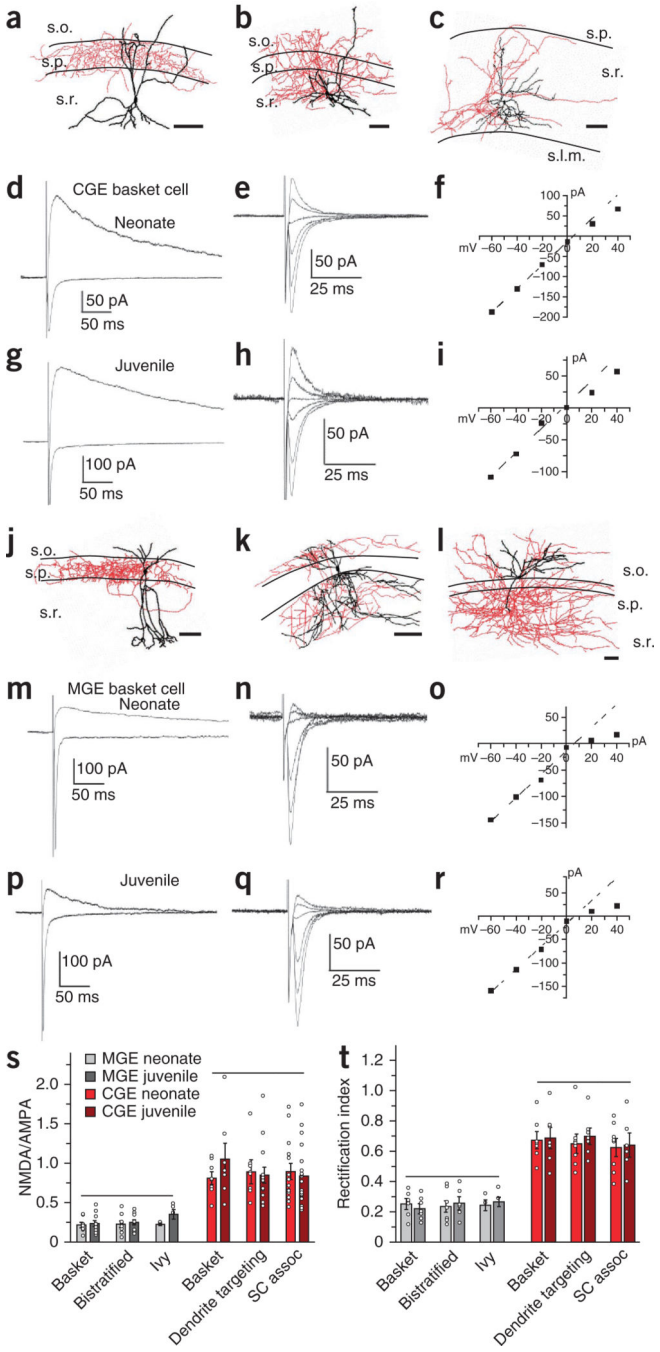

Figure 2. MGE and CGE specification of synaptic glutamate receptor expression is maintained through early development

(**a**–**c**) Representative reconstructions of a juvenile CGE-derived perisomatic-targeting basket cell (**a**), a wide-range dendrite-targeting cell (**b**) and a Schaffer collateral–associated cell (**c**). Somata and dendrites are shown in black, and axons are shown in red. Approximate boundaries of strata oriens, pyramidale and radiatum (s.o., s.p., and s.r., respectively) are drawn. Scale bars, 100 μm. (**d**–**f**) Representative EPSC profiles for CGE-derived interneurons from neonates (traces were from a CGE-derived basket cell). (**d**) Superimposed

averaged AMPAR-mediated EPSCs (V_h = −70 mV) and isolated NMDAR-mediated EPSCs (+40 mV; recorded in the presence of 5 μM NBQX). (**e**) AMPAR EPSC *I–V* relationship (V_h = −60 mV to +40 mV in 20-mV increments and in the presence of 100 μM AP5). (**f**) Plot of the *I–V* relationship for the AMPAR EPSC peak amplitude shown in **e**. (**g–i**) As in **d–f** but for a juvenile CGE-derived basket cell. (**j–l**) Reconstruction of a juvenile MGE-derived perisomatic basket cell (**j**), a bistratified cell (**k**) and an ivy cell (**l**). Scale bars, 100 μm. (**m–r**) Representative data from MGE-derived basket cells in neonates (**m–o**) and juveniles (**p–r**) as in **d–i**. (**s**) Summary histogram for the NMDAR-to-AMPAR ratios for anatomically confirmed neonate and juvenile MGE-and CGE-derived interneurons (MGE: basket neonate, 8 cells from 8 slices from 6 mice; basket juvenile, 11 cells from 11 slices from 9 mice; bistratified neonate, 9 cells from 9 slices from 6 mice; bistratified juvenile, 10 cells from 10 slices from 8 mice; ivy neonate, 4 cells from 4 slices from 4 mice; ivy juvenile, 5 cells from 5 slices from 5 mice; CGE: basket neonate, 8 cells from 8 slices from 7 mice; basket juvenile, 7 cells from 7 slices from 7 mice; dendrite-targeting neonate, 9 cells from 9 slices from 8 mice; dendrite-targeting juvenile, 14 cells from 14 slices from 12 mice; Schaffer collateral–associated (SC assoc) neonate, 14 cells from 14 slices from 12 mice; Schaffer collateral–associated juvenile, 19 cells from 19 slices from 19 mice). (**t**) Summary data for the rectification index of AMPAR-mediated EPSCs (MGE: basket neonate, 7 cells from 7 slices from 6 mice; basket juvenile, 7 cells from 7 slices from 7 mice; bistratified neonate, 8 cells from 8 slices from 6 mice; bistratified juvenile, 6 cells from 6 slices from 4 mice; ivy neonate, 4 cells from 4 slices from 4 mice; ivy juvenile, 5 cells from 5 slices from 5 mice; CGE: basket neonate, 7 cells from 7 slices from 5 mice; basket juvenile, 7 cells from 7 slices from 7 mice; dendrite-targeting neonate, 8 cells from 8 slices from 5 mice; dendrite-targeting juvenile, 7 cells from 7 slices from 7 mice; Schaffer collateral–associated neonate, 8 cells from 8 slices from 4 mice; Schaffer collateral–associated juvenile, 6 cells from 6 slices from 5 mice). One-way analysis of variance (**s**, d.f. = 11, F = 11.37; **t**, d.f. = 11, F = 18.7) and *post hoc* Tukey analysis were conducted to test for significant differences (P < 0.05) across means. Horizontal lines above the data indicate no significant difference. Group data are presented as mean ± s.e.m., with results from individual experiments represented by open circles.

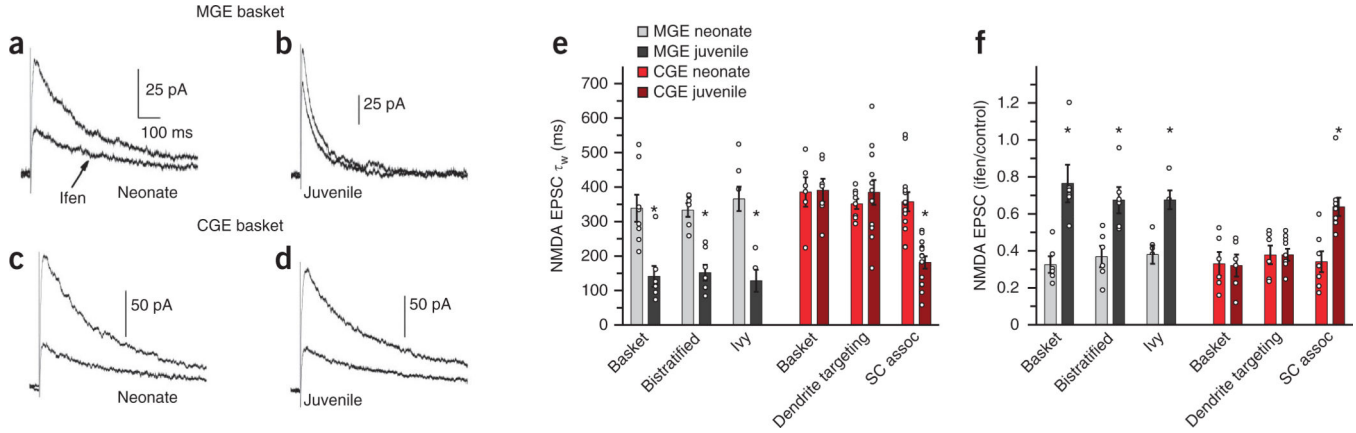

Figure 3. Developmental expression of synaptic GluN2 is cell-type specific

(**a**–**d**) Evoked Schaffer collateral NMDAR-mediated EPSCs in the absence or presence of ifenprodil (ifen; 5 μM) for representative MGE-derived basket cell (**a,b**) and a CGE-derived basket cell (**c,d**) from a neonate (**a,c**) and a juvenile (**b,d**). (**e**) Summary plot for the NMDAR EPSC decay kinetics weighted time constant (π_w) for both neonate and juvenile MGE- and CGE-derived interneurons (MGE, basket neonate, 8 cells from 8 slices from 6 mice; basket juvenile, 7 cells from 7 slices from 7 mice; bistratified neonate, 6 cells from 6 slices from 5 mice; bistratified juvenile, 7 cells from 7 slices from 5 mice; ivy neonate, 7 cells from 7 slices from 7 mice; ivy juvenile, 5 cells from 5 slices from 5 mice; CGE: basket neonate, 6 cells from 6 slices from 5 mice; basket juvenile, 7 cells from 7 slices from 7 mice; dendrite-targeting neonate, 8 cells from 8 slices from 5 mice; dendrite-targeting juvenile, 13 cells from 13 slices from 8 mice; Schaffer collateral–associated neonate, 12 cells from 12 slices from 8 mice; Schaffer collateral–associated juvenile, 13 cells from 13 slices from 8 mice). (**f**) Summary graph of the developmental regulation of ifenprodil sensitivity expressed as the ratio of the NMDAR EPSC peak amplitude measured in the presence of ifenprodil divided by the control NMDA EPSC peak amplitude (MGE, basket neonate, 6 cells from 6 slices from 5 mice; basket juvenile, 6 cells from 6 slices from 4 mice; bistratified neonate, 6 cells from 6 slices from 5 mice; bistratified juvenile, 6 cells from 6 slices from 5 mice; ivy neonate, 6 cells from 6 slices from 6 mice; ivy juvenile, 5 cells from 5 slices from 5 mice; CGE: basket neonate, 6 cells from 6 slices from 5 mice; basket juvenile, 6 cells from 6 slices from 6 mice; dendrite-targeting neonate, 6 cells from 6 slices from 5 mice; dendrite-targeting juvenile, 9 cells from 9 slices from 8 mice; Schaffer collateral–associated neonate, 6 cells from 6 slices from 5 mice; Schaffer collateral–associated juvenile, 8 cells from 8 slices from 8 mice). Unpaired *t* test was used for the comparisons between neonates and juveniles for each cell type (**e**, MGE: basket, $*P = 0.002$, d.f. = 13, $t = 3.9$; bistratified, $*P = 0.0001$, d.f. = 11, $t = 5.9$; ivy, $*P = 0.0005$, d.f. = 10, $t = 4.9$; CGE: basket, $P = 0.92$, d.f = 11, $t = -0.107$; dendrite targeting, $P = 0.49$, d.f. = 19, $t = -0.7$; Schaffer collateral associated, $*P = 9.9 \times 10^{-6}$, d.f. = 23, $t = 5.6$; **f**, MGE: basket, $*P = 0.001$, d.f. = 10, $t = -4.34$; bistratified, $*P = 0.004$, d.f. = 10, $t = -3.65$; ivy, $*P = 0.006$, d.f. = 9, $t = -4.55$; CGE: basket, $P = 0.91$, d.f = 10, $t = 0.118$; dendrite targeting, $P = 0.99$, d.f. = 13, $t = -0.01$; Schaffer collateral associated, $*P = 0.005$, d.f. = 12, $t = -3.39$). Group data are presented as mean ± s.e.m., with results from individual experiments represented by open circles.

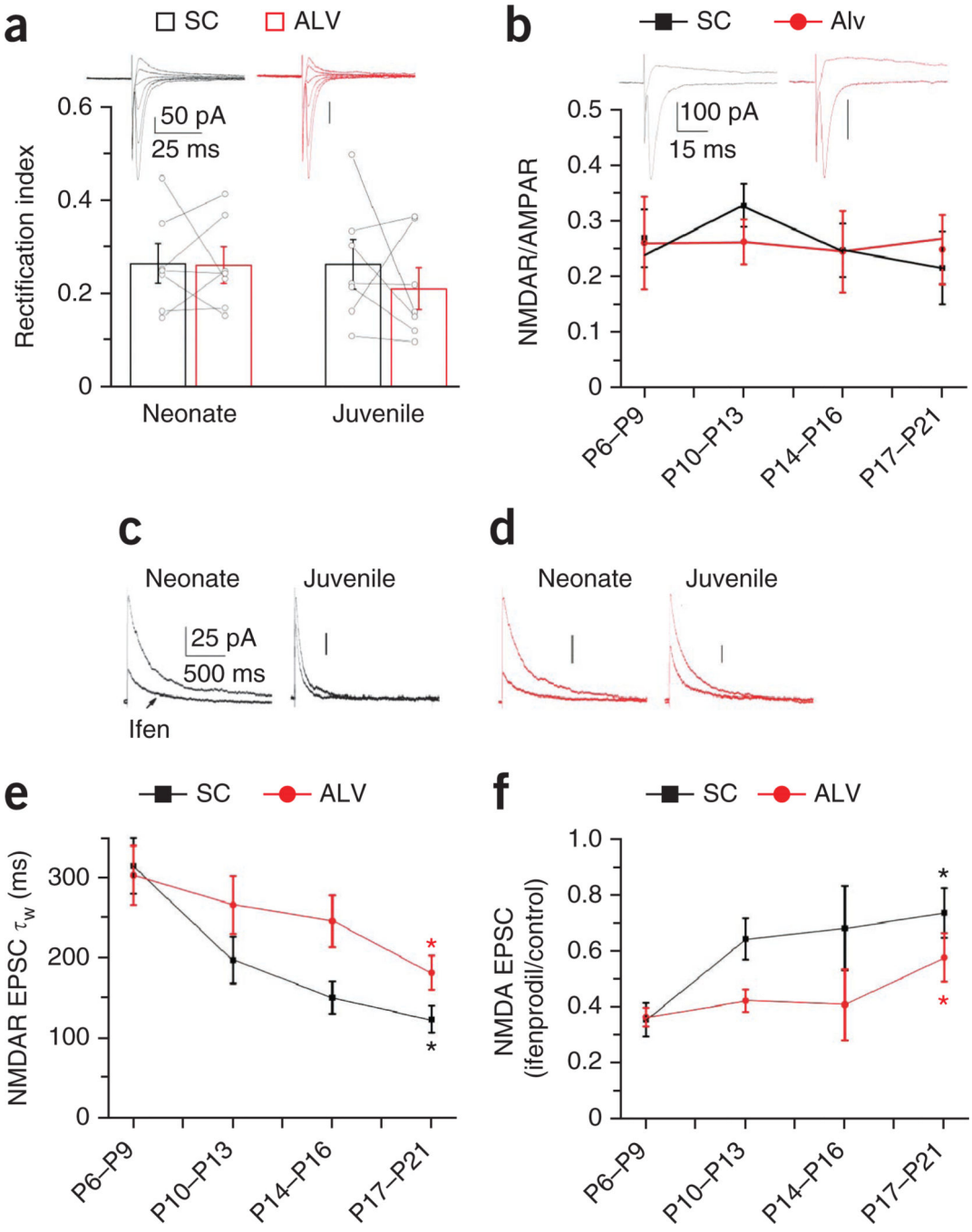

Figure 4. Afferent specificity of glutamatergic transmission maturation in MGE-derived cells

(**a**) AMPAR EPSC rectification index for Schaffer collateral inputs (black) and ALV inputs (red) onto identified MGE-derived basket and bistratified interneurons (pooled data). The histogram bars represent the mean data set, and open circles represent tethered Schaffer collateral and ALV individual data points from the same recording (neonate, 7 cells from 7 slices from 4 mice; juvenile: 7 cells from 7 slices from 3 mice). The upper traces show representative AMPAR *I–V* relationships of Schaffer collateral and ALV inputs onto a single MGE-derived basket cell (neonate, $P = 0.94$, d.f. = 6, $t = 0.08$; juvenile, $P = 0.44$, d.f.

= 6, t = 0.83; paired t test). Traces are on the same time scale, and the vertical bars represent 50 pA. (**b**) NMDAR-to-AMPAR ratio for Schaffer collateral and ALV inputs across four developmental time points. The upper traces show representative mean NMDAR-to-AMPAR currents evoked by Schaffer collateral and ALV inputs onto a single MGE-derived basket cell (P6–P9, 5 cells from 5 slices from 2 mice; P10–P13, 8 cells from 8 slices from 4 mice; P14–P16, 5 cells from 5 slices from 3 mice; P17–P21, 6 cells from 6 slices from 3 mice). Traces are on the same time scale, and the vertical bars represent 100 pA. (**c,d**) The developmental loss of ifenprodil sensitivity in NMDAR EPSCs at Schaffer collateral (black) and ALV (red) inputs in neonate and juvenile MGE-derived basket cells. Traces in **c** and **d** are on the same time scale, and the vertical bars represent 25 pA. (**e**) Summary plot of the developmental profile of NMDAR EPSC decay kinetics from Schaffer collateral and ALV inputs (*P = 0.0002, d.f. = 24, t = 4.4 for the Schaffer collateral input and *P = 0.0152, d.f. = 14, t = 2.77 for the ALV input for the comparison of the P17–P21 and P6–P9 data sets). (**f**) Summary plot for the developmental profiles of NMDA EPSC ifenprodil sensitivity from Schaffer collateral and ALV inputs (*P = 0.0002, d.f. = 26, t = 4.26 for the Schaffer input and *P = 0.0352, d.f. = 18, t = −2.28 for the ALV input for the comparison of the P17–P21 and P6–P9 data sets). (**e**, Schaffer collateral P6–P9, 19 cells from 19 slices from 12 mice; ALV P6–P9, 9 cells from 9 slices from 5 mice; Schaffer collateral and ALV P10–P13, 8 cells from 8 slices from 4 mice; Schaffer collateral and ALV P14–P16, 5 cells from 5 slices from 3 mice; Schaffer collateral P17–P21, 7 cells from 7 slices from 3 mice; ALV P17–P21, 7 cells from 7 slices from 4 mice; **f**, Schaffer collateral P6–P9, 19 cells from 19 slices from 12 mice; ALV P6–P9, 11 cells from 11 slices from 5 mice; Schaffer collateral and ALV P10–P13, 8 cells from 8 slices from 4 mice; Schaffer collateral and ALV P14–P16, 5 cells from 5 slices from 3 mice; Schaffer collateral P17–P21, 9 cells from 9 slices from 4 mice; ALV P17–P21, 9 cells from 9 slices from 4 mice.) Group data are presented as mean ± s.e.m., with results from individual experiments represented by open circles.

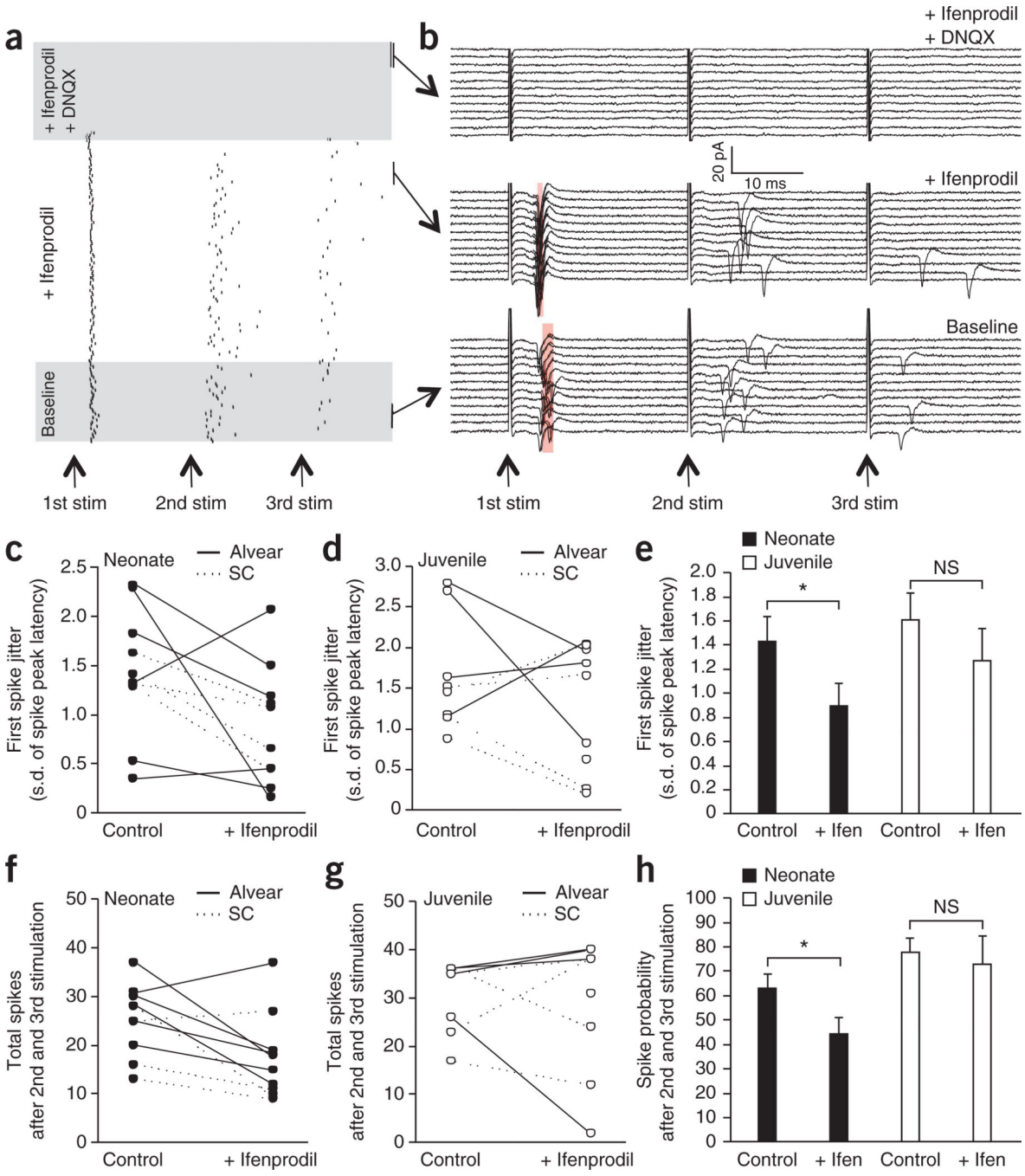

Figure 5. GluN2B-containing NMDARs participate in summation and spike timing of young MGE-derived interneurons

(**a**) Raster plot of a single representative cell-attached recording from a P6 MGE-derived interneuron demonstrating evoked spikes elicited by three stimuli given at a frequency of 40 Hz to the alvear path as indicated by the arrows (stim). The intersweep frequency was 0.1 Hz, and the numbers of sweeps were 30, 90 and 30 for the baseline, 5 μM ifenprodil and 5 μM ifenprodil plus 10 μM DNQX conditions, respectively. The conditions are delineated by shaded areas. (**b**) Raw traces of the same experiment as in **a** showing spiking of the neonate MGE-derived interneuron for 12 consecutive sweeps in each condition as indicated. Shaded

red regions indicate the s.d. of the spike peak latency. Arrows at the bottom show the time of each stimulus (stim) in the 40-Hz train. (**c**) Effect of ifenprodil on the jitter of the spike in an MGE-derived neonate interneuron (measured as the s.d. of the spike peak latency) evoked by the first stimulation in the 40-Hz train. (**d**) As in **c** but for juvenile MGE-derived interneurons. (**e**) Pooled data for the effects of blocking GluN2B by ifenprodil on spike jitter in both neonate and juvenile MGE-derived interneurons (neonate, **P* = 0.036, d.f. = 9, *t* = −2.28; juvenile, *P* = 0.18 (not significant (NS)), d.f. = 7, *t* = −1.17). (**f**) Effect of ifenprodil on the combined number of spikes after the second and third stimulation of the 40-Hz train in MGE-derived neonate interneurons. (**g**) As in **f** but for juvenile MGE-derived interneurons. (**h**) Pooled data for the effects of blocking GluN2B by ifenprodil on spike probability after the second and third spikes in the 40-Hz train in both neonate and juvenile MGE-derived interneurons (neonate, **P* = 0.024, d.f. = 9, *t* = −2.57; juvenile, *P* = 0.36 (NS), d.f. = 7, *t* = −0.73). In **c, d, f** and **g**, each pair of data points joined by a line depicts an individual experiment. Solid and dotted lines indicate synaptic-evoked spikes in MGE-derived interneurons after alvear and Schaffer collateral stimulation, respectively. For the pooled graphs in **e** and **h**, data from alvear and Schaffer collateral stimulation were combined (neonate, *n* = 10 cells recorded in 10 slices from 5 mice; juvenile, *n* = 8 cells recorded in 8 slices from 2 mice). Group data are presented as mean ± s.e.m.

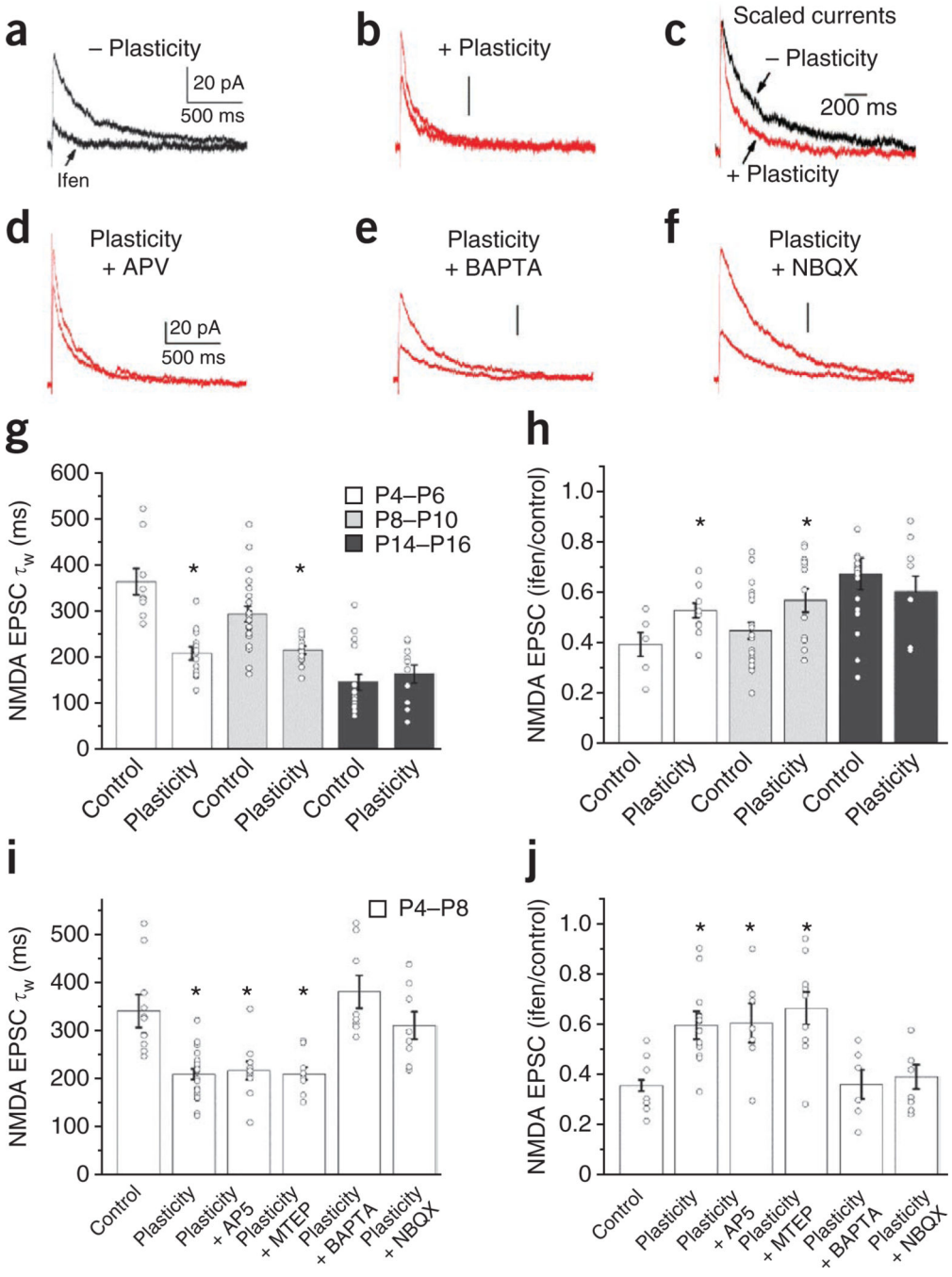

Figure 6. An activity-dependent change in GluN2 subunit expression in neonatal MGE-derived cells

(**a**) A representative control (−plasticity) isolated NMDAR-mediated EPSC in the absence or presence of ifenprodil from a neonate MGE-derived interneuron (V_h = +40 mV). (**b**) A representative NMDAR EPSC in the absence or presence of ifenprodil measured after repetitive synaptic activity (+plasticity = 2 Hz, 200 stimuli delivered at a holding potential of −70 mV). (**c**) Scaled NMDAR EPSCs from **a** and **b** before ifenprodil administration to emphasize the differences in decay kinetics in cells receiving the plasticity induction

paradigm. (**d**–**f**) The same synaptic induction paradigm evoked changes in NMDAR EPSC decay kinetics and ifenprodil sensitivity in the presence of AP5 (100 μM) but did not evoke GluN2 subunit plasticity when delivered in the presence of intracellular BAPTA (10 mM) or bath-applied NBQX (5 μM). (**g**) Summary graph of NMDAR EPSC decay kinetics for basal control conditions (P4–P6, 9 cells from 9 slices from 6 mice; P8–P10, 22 cells from 22 slices from 8 mice; P14–P16, 17 cells from 17 slices from 5 mice) and after repetitive synaptic activity (plasticity, P4–P6, 13 cells from 13 slices, from 7 mice; P8–P10, 13 cells from 13 slices from 6 mice; P14–P16, 10 cells from 10 slices from 6 mice) at the specified developmental periods (*$P = 3.5 \times 10^{-5}$, d.f. = 20, $t = 5.3$ for P4–P6; *$P = 0.002$, d.f. = 33, $t = 3.4$ for P8–P10; $P = 0.51$, d.f. = 25, $t = -0.66$ for P14–P16). (**h**) Summary graph of NMDAR EPSC ifenprodil sensitivity for basal control conditions (P4–P6, 6 cells from 6 slices from 6 mice; P8–P10, 22 cells from 22 slices from 8 mice; P14–P16, 16 cells from 16 slices from 5 mice) and after repetitive synaptic activity (P4–P6, 11 cells from 11 slices from 7 mice; P8–P10, 15 cells from 15 slices from 6 mice; P14–P16, 9 cells from 9 slices from 6 mice) at the specified developmental periods (*$P = 0.02$, d.f. = 15, $t = -2.6$ for P4–P6; *$P = 0.03$, d.f. = 35, $t = -2.2$ for P8–P10; $P = 0.48$, d.f. = 123, $t = 0.72$ for P14–P16). (**i**) Summary graph of NMDAR EPSC decay kinetics for basal control conditions and after repetitive synaptic activity in the absence (control, 11 cells from 11 slices from 8 mice; plasticity, 20 cells from 20 slices from 13 mice; *$P = 1.3 \times 10^{-5}$, d.f. = 29, $t = 5.23$) or presence of the NMDAR antagonist AP5 (100 μM; 10 cells from 10 slices from 4 mice; *$P = 0.002$, d.f. = 19, $t = -3.66$), the mGluR5 antagonist MTEP (10 μM; 10 cells from 10 slices from 3 mice; *$P = 5.1 \times 10^{-4}$, d.f. = 19, $t = 4.18$), BAPTA (intracellular 10 mM; 8 cells from 8 slices from 3 mice; $P = 0.37$, d.f. = 17, $t = -0.92$) or NBQX (5 μM; 8 cells from 8 slices from 3 mice; $P = 0.46$, d.f. = 17, $t = -0.75$). (**j**) Summary graph of NMDAR EPSC ifenprodil sensitivity under the same conditions as in **i** in the absence of inhibitors (control, 9 cells from 9 slices from 8 mice; plasticity, 15 cells from 15 slices from 13 mice; *$P = 3.2 \times 10^{-4}$, d.f. = 22, $t = -4.26$), or in the presence of AP5 (100 μM; 7 cells from 7 slices from 4 mice; *$P = 0.005$, d.f. = 14, $t = 3.31$), MTEP (10 μM; 9 cells from 9 slices from 3 mice; *$P = 0.001$, d.f. = 16, $t = -3.97$), BAPTA (intracellular 10 mM; 6 cells from 6 slices from 3 mice; $P = 0.94$, d.f. = 13, $t = 0.072$) or NBQX (5 μM; 8 cells from 8 slices from 3 mice; $P = 0.57$, d.f. = 15, $t = -0.58$). Traces in **a,b** and **d**–**f** are all on the same time scale, and the vertical bar in each panel represents 20 pA, as illustrated in **a** and **d**. Unpaired *t* test was used for the comparisons of the various conditions to the basal control NMDA EPSCs. Group data are presented as mean ± s.e.m., with the results from individual experiments represented by open circles.

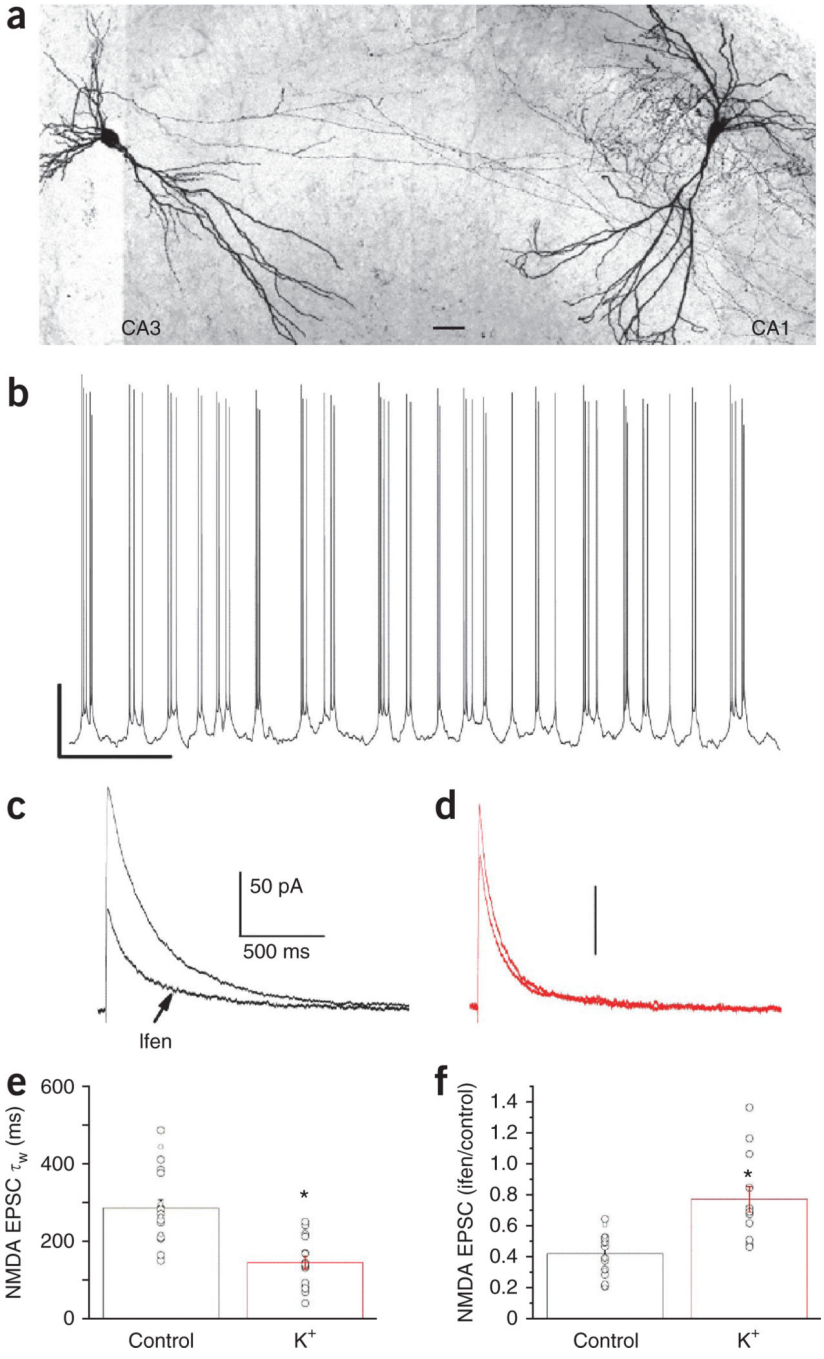

Figure 7. Principal-cell bursting activity in CA3 evokes a rapid GluN2 subunit switch in MGE-derived neonatal basket and bistratified cells

(**a**) A confocal image (×20) of a biocytin-filled CA3 pyramidal cell and a CA1 basket cell to illustrate the typical experimental recording configuration. (The confocal image was converted to grayscale and the color was inverted; scale bar, 60 μm.) (**b**) Whole-cell recording from a CA3 pyramidal cell to establish repeated robust bursting activity in the presence of elevated amounts of extracellular potassium (5 mM). After 5–8 min of monitoring CA3 bursting activity, the whole-cell configuration is established in an MGE-

derived interneuron. Scale bar, 20 mV/3 s. (**c,d**) Representative NMDA EPSCs and their ifenprodil sensitivity for neonate MGE-derived basket cells in control slices (**c**, black) and slices treated with a high-potassium (K^+) solution to promote CA3 pyramidal neuron burst firing (**d**, red). Traces in **c** and **d** are on the same time scale, and the vertical bars represent 50 pA, as indicated in **c**. (**e,f**) Summary plots for MGE-derived basket and bistratified cell NMDA EPSC decay kinetics (**e**; control, 19 cells from 19 slices from 14 mice; K^+, 17 cells from 17 slices from 8 mice; $^*P = 5.3 \times 10^{-6}$, d.f. = 34, $t = 5.39$) and ifenprodil sensitivity (**f**; control, 19 cells from 19 slices from 14 mice; K^+, 14 cells from 14 slices from 8 mice; $^*P = 7.8 \times 10^{-4}$, d.f. = 31, $t = -3.73$) recorded in control and K^+-treated slices. Group data are presented as mean ± s.e.m., with results from individual experiments represented by open circles.